The sugar-beet cyst nematode effector *Hs*2B11 targets the Arabidopsis serine protease inhibitor *At*PR-6 to favor parasitism

Joffrey Mejias[1,2], Melissa Bredow[1,2]*, Anil Kumar[1]*, Parijat S. Juvale[1,3], Thomas M. Maier[1], Ekkachai Khwanbua[1], Steven A. Whitham[1], Sebastian Eves-van den Akker[4] and Thomas J. Baum[1$]

[1] Department of Plant Pathology, Entomology and Microbiology, Iowa State University, Ames, Iowa, 50011, USA.

[2] Current Address: CIRAD, INRAE, UMR PHIM, Montpellier, France

[3] Current Address: BASF, Research Triangle Park, North Carolina, USA

[4] The Crop Science Centre, Department of Plant Sciences, University of Cambridge, Cambridge CB2 3EA, UK

[$]Corresponding author: Thomas J. Baum (tbaum@iastate.edu)

*authors contributed equally to this work

ORCIDs

Joffrey Mejias	0000-0001-7663-0314
Melissa Bredow	0000-0002-5564-9646
Anil Kumar	0000-0003-4101-9974
Parijat S. Juvale	0000-0003-2700-2359
Ekkachai Khwanbua	0009-0007-4013-941X
Steven A. Whitham	0000-0003-3542-3188
Sebastian Eves-van den Akker	0000-0002-8833-9679
Thomas J. Baum	0000-0001-9241-3141

Keywords: cyst nematode, *Heterodera schachtii*, effector, *Arabidopsis thaliana*, Pathogenesis-Related protein, protease inhibitor.

Abstract

Cyst nematodes secrete effector proteins to manipulate host cell biology and suppress immunity, yet the mechanisms underlying these interactions remain largely unexplored. In this study, we characterize the function of *Hs*2B11, a *Heterodera schachtii* effector that was previously shown to be expressed in the dorsal gland of sugar-beet cyst nematodes (BCN). Here, we report that in *Arabidopsis thaliana Hs2*B11 functions as an immune regulator that modulates the production of elicitor-induced oxidative species, likely to favor parasitism. To elucidate the molecular basis of this immune suppression, we performed a yeast-two-hybrid screen and identified the host serine protease inhibitor *At*PR-6 as a direct interactor of *Hs*2B11. We show that *At*PR-6 acts as a positive regulator of plant immunity; its expression is induced upon nematode infection and knock-out of *AtPR-6* compromises oxidative species production leading to higher susceptibility to *H. schachtii* infection. Conversely, *AtPR-6* overexpression enhances immune responses resulting in increased resistance to BCN infection. Detailed analysis of this interaction demonstrated that *Hs*2B11 interacts with *At*PR-6 using its carboxyl-terminal domain. AlphaFold2 predicts that the C-terminal domain forms a beta-solenoid-like structure with a ladder of serine residues organized across one of its surfaces. We propose that using this interface, *Hs*2B11 targets *At*PR-6 via molecular titration, preventing the inhibitor from regulating host proteases that control immune signaling. These findings highlight a counter-defense strategy where a nematode effector neutralizes a specific host protease inhibitor to subvert plant immunity.

Introduction

Soybean (*Glycine max*) is one of the most important sources of food and feed production in the world [1]. Importantly, as soybean forms symbiotic relationships with nitrogen-fixing bacteria, its cultivation reduces the need for exogenous fertilizer applications, supporting sustainable agriculture practices [2]. The most destructive pathogen of soybean is the soybean cyst nematode (SCN), *Heterodera glycines*, which causes yield losses estimated to be billions of dollars each year [3]. To maintain soybean crops at their highest production level, it is crucial to identify novel resistance sources or mechanisms that can be exploited to combat this pathogen.

SCN infects soybean by delivering effector molecules to hijack the plant's physiology, including a complete reprogramming of a selected root cell and the inactivation of plant defense mechanisms [4]. The sugar-beet cyst nematode (BCN), *H. schachtii,* is an effective model for studying cyst nematode pathogenicity, as it infects the model plant *Arabidopsis thaliana* (hereinafter, Arabidopsis). Cyst nematodes are attracted to host roots through chemoattraction and invade them to migrate into the vascular cylinder, inducing the formation of a reprogrammed feeding structure called a syncytium. The formation of this feeding structure allows nematodes to switch to a sedentary lifestyle and feed exclusively on those newly formed cell types. Through its nutrient and energy acquisition from the host, nematodes molt several times to become a female able to produce hundreds of eggs. The female will subsequently die and harden to form a "cyst" containing the eggs. Finally, new juveniles will hatch from those eggs when environmental conditions are favorable [5].

73 The plant immune system needs to be drastically suppressed during the entire life
74 cycle of the nematode, including penetration and formation of the feeding site.
75 Proteinaceous effectors are keystones of pathogenicity and essential to manipulate plant
76 physiology [6]. BCNs produce hundreds of secreted effector proteins, primarily in the
77 salivary glands, which are composed of two subventral gland cells and one dorsal gland
78 cell in cyst-nematodes. The subventral glands are involved in the production of secreted
79 cell-wall modifying enzymes that aid the migration of nematodes into the root. The dorsal
80 gland becomes more active at parasitic stages of infection and is mostly involved in the
81 production of effector proteins that suppress plant immunity, or initiate and maintain the
82 syncytium. Investigating the function of effectors capable of suppressing plant defenses,
83 and identifying their plant targets, could pinpoint key resistance genes or susceptibility
84 genes that can be engineered to create durable resistance against cyst-nematodes [7].

85 Among the large range of functions associated with effector proteins, those harboring
86 protease activity have been shown to be critical for pathogenicity. Secreted proteases
87 possessing virulence activity have been described for phytopathogenic bacteria, fungi,
88 viruses and nematodes [8–11], suggesting that proteases are used as common weapons
89 to favor infection. The effector AvrPphB, from *Pseudomonas syringae,* is one the most
90 characterized secreted protease effectors, which specifically targets a subfamily of
91 receptor-like cytoplasmic kinases to suppress defense responses induced by cell surface-
92 localized plant immune receptors such as FLAGELLIN SENSITIVE 2 (FLS2) [12].
93 Arabidopsis or soybean carrying the intracellular nucleotide-binding leucine-rich repeat
94 (NLR) protein RPS5 (RESISTANCE TO PSEUDOMONAS SYRINGAE 5) indirectly detect
95 AvrpPhB, by detecting the cleavage product of the Arabidopsis protein kinase AvrpPhB-

96 Susceptible 1, leading a hypersensitive cell death response, and resistance against *P.*
97 *syringae* [13]. Numerous proteases have been detected in the transcriptome or
98 secretome of phytoparasitic nematodes, underscoring their importance during interaction
99 with host plants [14–16]. In phytoparasitic nematodes, secreted proteases have been
100 proposed to function in helping to digest the intracellular contents of plant cells, which are
101 thereafter used as a nutrient source, or to hijack host proteins [14–16]. For example, the
102 SCN effector Cysteine Protease 1 (CPR1) targets a branched-chain amino acid
103 aminotransferase from soybean enhancing susceptibility to SCN [17].

104 In order to counteract the effect of secreted protease effectors, plants produce
105 protease inhibitors, some of which have been demonstrated to localize to the extracellular
106 space of plant cells to covalently link and inhibit pathogen secreted proteases. For
107 example, the activity of two subtilisin-like and trypsin-like proteases from *Fusarium*
108 *culmorum* are inhibited by three barley (*Hordeum vulgare*) chymotrypsin/subtilisin
109 protease inhibitors, CI-1A, -1B, and -2 [18]. Similarly, a trypsin-chymotrypsin protease
110 inhibitor from broad bean (*Vicia faba*) has demonstrated antifungal activity against
111 *Mycosphaerella arachidicola*, *F. oxysporum*, and *Botrytis cinerea* [19].

112 Protease inhibitors also directly modulate plant immunity by fine-tuning the activity of
113 endogenous plant proteases. For example, microbe-associated molecular pattern
114 (MAMP)-induced oxidative species production is tightly controlled by the activity of a
115 papain-like cysteine protease, XYLEM CYSTEINE PEPTIDASE 1 (XCP1), and its
116 inhibitor CYSTATIN 6 (CYS6) in Arabidopsis [20]. Alternatively, pathogens can secrete
117 protease inhibitors to target plant proteases such as the cysteine-protease inhibitor Avr2
118 from *Cladosporium fulvum* that binds and inhibits the tomato (*Solanum lycopersicum*)

119 cysteine protease Rcr3pim [21]. This interaction is sensed by the extracellular immune
120 receptor Cf-2, which is required to mount an immune response against this pathogen.
121 Comparatively less is known about protease control in plant-nematode interactions, with
122 only two examples of plant protease inhibition-driven defense being described, although
123 the effectors involved do not contain classical protease inhibitor domains [22,23].

124 We previously identified 18 novel SCN effector candidates through transcriptome
125 mining using isolated dorsal glands of *H. glycines* and confirmed their expression in the
126 salivary glands by *in situ* hybridization [24]. In the present study, we performed a
127 functional analysis of the *H. schachtii* homolog of one of these candidate effectors,
128 *Hs*2B11, and demonstrate that this effector modulates host immunity. We identified the
129 Arabidopsis Pathogenesis-Related (PR) protein *At*PR-6 (At2g38870), a plant serine
130 protease inhibitor, as an interactor of *Hs*2B11. This interaction was confirmed by split-
131 luciferase assays and bimolecular fluorescent complementation. We show that *At*PR-6
132 acts as a positive regulator of immunity involved in defense against BCN. Moreover, we
133 identify potential host interactors of *At*PR-6, including plant serine proteases. Our results
134 suggest that *At*PR-6 controls basal immunity through the inhibition of plant serine
135 proteases and/or secreted nematode effectors. This study demonstrates, for the first time,
136 that a cyst-nematode effector targets a protease inhibitor to favor parasitism. These
137 results strengthen our knowledge of plant defense through protease inhibition and
138 suggest that nematodes could counter these defenses through titration of serine protease
139 inhibitors.

140

141

142 ## Results

143 ### *Hs*2B11 is a novel effector carrying a unique carboxyl-terminal domain

144 Bioinformatic analysis of *Hs*2B11 (Hsc_gene_18368) indicates that the gene encodes a
145 putative *H. schachtii* secreted effector with high similarity to GLAND7 (*Hg*2B11; GenBank
146 ID: KJ825718), sharing 85.3% identity at the amino acid level (Fig 1A). We previously
147 localized the expression of GLAND7 transcripts to the dorsal gland of parasitic juveniles
148 using *in situ* hybridization [24]. *Hs*2B11 is also highly expressed in the dorsal gland in
149 transcriptomic analyses conducted on isolated salivary glands (Fig 1B; [25]), and
150 transcripts have been identified during early infection in life cycle RNA-seq analysis data
151 (Fig 1C; [26]). These results suggest that *Hs*2B11 is a secreted effector important for early
152 infection. A BLAST search against WormBase Parasite indicates that this effector is only
153 present in the *H. schachtii* and *H. glycines* genomes and not in closely-related cyst
154 nematodes from the *Globodera* genus, suggesting that this gene has evolved recently.
155 Notably, a cluster of genes encoding paralogues of *Hs*2B11 is present on chromosome
156 2, suggesting their importance in the infection process (Fig 1D; Fig S1).

157 The *Hs*2B11 gene was cloned from cDNA collected from parasitic juveniles,
158 corresponding to Hsc_18368 [25]. *Hs*2B11 is a 366 amino acid protein that possesses a
159 predicted secretion signal peptide (according to SignalP analysis; Fig 1A) and lacks a
160 transmembrane domain (according to Phobius analysis). Both *Hs*2B11 and *Hg*2B11
161 contain two distinct domains, an N-terminal domain with no notable features, and a C-
162 terminal domain that consists of a number of alternating repetitive sequences (Fig 1A; Fig
163 1E). To explore the significance of this repetitive region, we used Alphafold2 based on

164 colab design [27] to predict its 3D structure (Fig 1E). Even though this software is better
165 suited to predicting already described domains, it predicts a beta-solenoid-like structure
166 stabilized by a hydrophobic core with high confidence (pLDDT score >90). Beta solenoids
167 are a protein fold composed of repeating beta strands, arranged in anti-parallel fashion
168 to form a superhelix. Each repetitive sequence of the C-terminal domain forms one loop,
169 repeating ten times. Interestingly, this structure harbors a serine ladder on one edge, and
170 a ladder of alternating acidic and basic amino acids (asparagine, aspartate, arginine and
171 lysine residues) on another edge, exposing clear polar interaction surfaces (Fig 1E). We
172 ran this structure through the FoldSeek database [28] and obtained significant hits for
173 beta-solenoids, however, these structures varied in the length of repetitive sequences
174 and did not possess the same laddering effect of outward-facing residues on their
175 surfaces, emphasizing the unique structure of this *Hs*2B11 effector.

176

177 **_Hs_2B11 localized to the cytoplasm and the endoplasmic reticulum when**
178 **transiently expressed in _Nicotiana benthamiana_**

179 To gain insight into cellular function of *Hs*2B11, we first studied its subcellular localization
180 *in planta*. We used transient expression in *N. benthamiana* leaves to express GFP fusion
181 constructs with *Hs*2B11 without its endogenous signal peptide and monitored localization
182 using confocal microscopy (Fig 2A). Our observations revealed that the GFP-*Hs*2B11
183 fusion exhibited a nucleo-cytoplasmic distribution, whereas the *Hs*2B11-eGFP fusion was
184 primarily localized in the endoplasmic reticulum (ER) and the cytoplasm. We validated
185 the ER localization pattern by co-expressing *Hs*2B11-GFP with the ER subcellular marker
186 AtWAK2-mCherry-HDEL (Fig 2B).

187 **Expression of *Hs*2B11 in Arabidopsis displays contrasting phenotypes correlated**
188 **with expression levels**

189 In order to assess if *Hs*2B11 dampens host immunity to promote parasitism we generated
190 two independent Arabidopsis lines (1-3-3 and 14-3-4) expressing the effector under the
191 control of a 35S promoter (Fig 3A). qRT-PCR analysis confirmed the expression of
192 *Hs*2B11 in both transgenic lines (Fig 3B). Line 14-3-4 moderately expressed *Hs*2B11
193 while line 1-3-3 showed approximately three times higher expression (Fig 3B).
194 Interestingly, moderate expression of *Hs*2B11 resulted in larger rosettes compared to Col-
195 0 plants at 2- and 5-weeks post-germination (wpg) (Fig 3A). In contrast, line 1-3-3, which
196 displayed stronger *Hs2B11* expression, perturbed the growth of rosettes compared to
197 Col-0 and caused spontaneous lesions in leaves (Fig 3A). Consistent with our
198 observations of above-ground growth phenotypes, the highly expressing line (1-3-3)
199 displayed perturbed root growth when grown on MS medium, although no difference in
200 root length was observed in the moderately expressing line (14-3-4) compared to the Col-
201 0, under these conditions (Fig 3C-D). In order to assess the potential role of *Hs*2B11 in
202 immune suppression, we monitored the production of oxidative species in transgenic
203 *Hs*2B11-expressing Arabidopsis lines in response to flg22, an immunogenic peptide
204 derived from bacterial flagellin. We observed that the moderately expressing-*Hs*2B11 line
205 shows a dampened oxidative species burst, whereas the higher expressing-*Hs*2B11 line
206 shows higher oxidative species production (Fig 3E). In contrast, heterologous expression
207 of *Hs*2B11 in Arabidopsis did not impact BCN infection (Fig 3F). As *Hs*2B11 (Fig 1C) and
208 related paralogs (Fig S1) are highly expressed during early infection, we speculate that
209 additional expression in Arabidopsis likely has no observable effect on infection.

210 Together, our results suggest that *Hs*2B11 plays an important role in modulating host
211 defense responses. However, the contrasting immune and physiological phenotypes
212 observed in our two transgenic lines indicates that *Hs*2B11 could interact with plant
213 processes that interplay between defense and growth, in a dose-dependent manner.

214

215 **_Hs_2B11 interacts with an Arabidopsis PR-6 protein in yeast and _in planta_**

216 In order to gain a better understanding of how *Hs*2B11 is regulating plant defense
217 responses, we sought to identify host interacting proteins by conducting three
218 independent yeast-two hybrid (Y2H) screens against Y2H libraries generated from 3, 7,
219 and 10 dpi BCN-infected Arabidopsis. Screening against the 3-dpi cDNA library yielded
220 20 potential interacting proteins (Fig 4A; Supplemental File 1). Among these candidate
221 interactors, we identified the Pathogenesis-Related family 6 protein (*At*PR-6;
222 AT2G38870) that was captured 11 times. Using the 7 dpi and 10 dpi libraries, we identified
223 17 and 26 unique interacting proteins, respectively (Fig 4A; Supplemental File 1). Notably,
224 *At*PR-6 was the only protein to be captured in all three of these screens (Fig 4A). *At*PR-
225 6 belongs to a conserved family of six proteins in Arabidopsis [29], three of which
226 (AT2G38870, AT5G43570 and AT5G43580) are upregulated during BCN infection at 10
227 dpi (Fig S2). Nevertheless, only one gene (AT2G38870) was identified in our screen.
228 AlphaFold2 predicts that all *At*PR-6 proteins possess a highly conserved C-terminal
229 protease inhibitor domain (Fig S2). In contrast, the N-terminal extension domains were
230 distinct across the six members, which could provide specificity for certain proteases and
231 interactors such as *Hs*2B11.

232 The *At*PR-6 protein family is upregulated in response to biotic stresses, including
233 infection with fungal pathogens [30], exposure to SCN [31], and elicitation with flg22 or
234 the damage-associated molecular pattern (DAMP) *At*Pep1 in roots [32]. *At*PR-6
235 (AT2G38870) expression has been associated with resistance to *B. cinerea [*30] and *F.*
236 *graminearum [*33], however, *At*PR-6 has no demonstrated role in nematode defense.
237 Plant extracts containing diverse protease inhibitors were previously shown to inhibit
238 trypsin or subtilases (serine proteases) from various phytopathogen origins such as
239 *Alternaria alternata*, *F. oxysporum* and *B. cinerea* [34]. We therefore aimed to further
240 characterize the role of *At*PR-6 in pathogen defense and its interaction with the effector
241 *Hs*2B11.

242 We first validated the interaction between *Hs*2B11 and *At*PR-6 using pairwise Y2H
243 analysis (Fig 4B). To determine more specifically the site of interaction between these
244 proteins, we generated N- and C-terminal truncation mutants of *Hs*2B11, corresponding
245 to the domains outlined in Fig 1A. We observed that only the C-terminal repetitive domain
246 of *Hs*2B11 is required for interaction with *At*PR-6 and that the N-terminal domain alone is
247 not capable of interacting with this protein. We further confirmed that the C-terminal
248 domain of *Hs*2B11 is uniquely required for association with *At*PR-6 by performing split-
249 luciferase complementation assays in *N. benthamiana* leaves. In agreement with our Y2H
250 analysis, *Hs*2B11 and *At*PR-6 strongly interact *in planta* (Fig 4C). Notably, there was
251 reduced interaction with the C-terminal domain, compared to the full-length *Hs*2B11
252 protein, which could indicate that the N-terminal domain partially facilitates interaction
253 between these proteins. Given the repetitive nature of this effector, we were curious if
254 only a subset of these C-terminal repeats is required for interaction. We therefore

255 additionally generated *Hs*2B11 truncation mutants consisting of 2 or 4 repeats,
256 2R_*Hs*2B11 and 4R_*Hs*2B11, respectively. Indeed, *At*PR-6 associated with both
257 2R_*Hs*2B11 and 4R_*Hs*2B11 (Fig 4B). Together, these results indicate that *Hs*2B11
258 strongly associates with *At*PR-6 through interaction with its C-terminal domain.

259

260 **_Hs_2B11 and _At_PR-6 interact in the nucleus, cytoplasm and endoplasmic reticulum**

261 To gain insight into the biological relevance of this interaction we conducted bimolecular
262 fluorescence complementation (BiFC) assays to determine the site of interaction of these
263 proteins *in planta*. We identified a strong signal in the ER and cytoplasm of *N.*
264 *benthamiana* leaf cells transiently expressing *Hs*2B11 and *At*PR-6 possessing N- or C-
265 terminal split-YFP fusions (Fig 4D; Fig S3) which co-localized with the ER marker,
266 AtWAK2 (Fig S4). We performed these assays using a BiFC vector that co-expresses a
267 CFP-tagged Golgi marker in order to confirm the expression of our genes in the absence
268 of YFP re-constitution (Fig 4D). Expression of RFP-*At*PR-6 or *At*PR-6-RFP fusions in *N.*
269 *benthamiana* resulted in a nucleo-cytoplasmic and nucleo-cytoplasmic/ER localization
270 pattern, respectively (Fig 5). To investigate whether *Hs*2B11 and *At*PR-6 co-localized in
271 the same subcellular compartment, we co-expressed GFP fusions of *Hs*2B11 along with
272 RFP fusions o*f At*PR-6 and observed that they indeed co-localized in the nucleo-cytosolic
273 compartment and/or the ER, depending on the orientation of the tags used (Fig 5).

274

275

276

277 ***At*PR-6 is upregulated in early syncytia**

278 To investigate the spatio-temporal expression pattern of the *AtPR-6* gene in response to
279 BCN infection, we generated a transcriptional fusion of the 846 bp sequence upstream of
280 the AT2G38870 start codon with the GUS reporter gene (p*AtPR6:GUS*) and produced
281 stable Arabidopsis lines. We performed histochemical GUS assays and found that the
282 *AtPR-6* promoter is active ubiquitously in leaves, trichomes, and roots in the absence of
283 BCN infection, with a stronger expression in the root elongation zone and no expression
284 in the root tip (4 h incubation with X-Gluc) (Fig S5). In order to distinguish changes in
285 expression associated with BCN infection, we repeated these assays using a shorter
286 substrate incubation period (30 min in the presence of X-Gluc). We observed a similar
287 expression pattern in these experiments (Fig 6A-D). We next infected these Arabidopsis
288 lines with *H. schachtii* and monitored GUS expression using this shorter incubation time
289 at 4 dpi and 14 dpi (Fig 6E-H). We observed an upregulation of *At*PR-*6* promoter-driven
290 expression in syncytia at 4 dpi (Fig 6E, 6F) but not at 14 dpi (Fig 6G, 6H), indicating that
291 this gene is upregulated as an early response to BCN infection. This observation is in line
292 with previously established RNA-seq data that indicate an upregulation of *AtPR-6* during
293 early infection with an expression peak at 10 hpi with BCN ([25]; Fig S2).

294

295 ***At*PR-6 is a positive regulator of early immune signaling and provides resistance**
296 **to *H. schachtii***

297 Given that our and previous data indicate that *AtPR-6* is responsive to infection and
298 elicitation with immunogenic peptides, it is reasonable to expect the gene has a role in

299 regulating host defense responses. We therefore obtained a T-DNA knockout line of
300 *AtPR-6* (SALK_111051C) (Fig 7A) and conducted infection assays with *H. schachtii*. The
301 *AtPR-6* knockout line was more susceptible to BCN infection, displaying a significantly
302 higher number of cysts per plant compared to wild-type Col-0 plants (Fig 1B). To
303 determine if *AtPR-6* is more generally involved in basal defense, we monitored flg22-
304 induced oxidative species production, which showed a reduced immune response (Fig
305 1C). Since only one line was available with a T-DNA insertion in the coding region of
306 *At*PR-6, we additionally generated *At*PR-6 overexpression lines driven by a 35S promoter
307 and confirmed *AtPR-6* overexpression by RT-qPCR analysis (Fig 7D). Consistently,
308 *At*PR-6 overexpression lines were more resistant to BCN infection, displaying significantly
309 reduced cysts per plant compared to wild-type Col-0 controls (Fig 1E). Overexpression of
310 *At*PR-6 also correlated with an overproduction of oxidative species in response to flg22
311 (Fig 1F). Together, our data provide direct evidence for a role of *At*PR-6 in immune
312 signaling and defence against *H. schachtii.*

313

314 **_At_PR-6 interacts with plant serine proteases in Y2H**

315 Since little is known about the function of the *At*PR-6 protein encoded by the AT2G38870
316 gene, we performed a Y2H screen to identify plant interacting proteins. We used *At*PR-6
317 as bait against a mix of the three cDNA libraries used previously and identified a total of
318 25 potential targets (Table S1). Among these proteins, we captured two extracellular plant
319 serine proteases (AT1G20160 and AT3G14240), supporting the role of *At*PR-6 as a
320 serine protease inhibitor. Since the cDNA libraries have been prepared from BCN-
321 infected Arabidopsis roots, we also captured three proteins from the nematode, among

322 which were two protein-encoding genes with predicted secretion signal peptides
323 (Hsc_13411 and Hs_G3197) (Table S1). Although these genes are not predicted to
324 encode proteins possessing protease activity, one of these genes (Hsc_20080) is a
325 transthyretin-like protein, which shares similarity to transthyretin proteins that have been
326 demonstrated, in some cases, to possess cryptic serine protease activity [35]. Our data
327 suggest that *At*PR-6 could target both host and nematode serine proteases, in an
328 interplay with growth and defense to counteract nematode infection.

329

330 ## Discussion

331 In this study, we functionally characterized *Hs*2B11, a previously uncharacterized BCN
332 effector gene from *H. schachtii*. *Hs*2B11 is one of the multiple pioneer genes that have
333 no described function in the *H. schachtii* genome. Since the *Heterodera* genera have
334 evolved sophisticated relationships with their hosts through the formation of a peculiar
335 feeding site and a narrow host range [36], it is not surprising to find that many pioneer
336 genes have still not been functionally investigated. Multiple paralogues of *Hs*2B11 are
337 found in the genome of *H. schachtii* suggesting that these genes could act redundantly,
338 or have diversified to target a larger range of host targets. Moreover, *Hs*2B11 is an
339 orthologue of GLAND7 and shows sequence and structural similarity to G15A10, an
340 effector also identified in the dorsal gland of SCN [24]. Given that these genes have not
341 been identified outside of the *Heterodera* genera, we speculate that this gene family has
342 evolved recently to act on plant processes related to *Heterodera* cyst nematode infection
343 strategies. Here, we demonstrate that *Hs*2B11 perturbs flg22-induced oxidative species

344 production in Arabidopsis, indicating a role in modulating basal defense responses. We
345 identified an *At*PR-6 protein, belonging to a family of serine protease inhibitors, as an
346 interactor of *Hs*2B11, which positively regulates basal immunity and defense against BCN
347 infection. Our data suggest that *Hs*2B11 targets *At*PR-6 to suppress its endogenous
348 immune functions.

349 In order to establish a role for *Hs*2B11 in plant parasitism, we generated 35S-
350 driven overexpression lines in Arabidopsis. During the course of experiments, we
351 observed that the level of *Hs2B11* expression in these transgenic lines caused reciprocal
352 phenotypes, with "lower" expression dampening defense and promoting plant growth, and
353 "higher" expression inducing basal defense responses and perturbed plant growth. These
354 results clearly demonstrate a role for *Hs*2B11 in regulating host defense responses that
355 seems to be intricately intertwined with plant growth. This growth-defense trade-off could
356 be the result of targeting a plant protein that interplays between these two processes.
357 This type of expression-dependent reciprocity has been documented previously in the *H.*
358 *schachtii*-Arabidopsis pathosystem. Low expression of the *H. schachtii* effector 32E03
359 was shown to inhibit the activity of the histone deacetylase HDT1, causing increased
360 acetylation of histone H3 along the rDNA chromatin, whereas higher expression triggered
361 repression of the same rDNA region [37]. Higher expression also resulted in dramatically
362 smaller plants which were more resistant to BCN infection, whereas lower expression
363 caused no obvious growth defects and higher susceptibility to infection. During a natural
364 infection, effector secretion is tightly regulated to precisely control the quantity and
365 location of specific sets of effectors in the host to optimally promote parasitism. Although
366 ectopic expression of effectors using transgenic systems can provide clues about the

367 function of a potential effector, it does not always reflect its real effect during physiological
368 conditions. We expect that *H. schachtii* would secrete *Hs*2B11 as a means of promoting
369 infection, leading us to hypothesize that the moderately expressing line is the most
370 representative of what would occur during BCN infection. Notably, we did not observe
371 any growth phenotype of *At*PR6 overexpression lines or of the *Atpr6* knockout line,
372 suggesting that *Hs*2B11 could have additional targets with developmental roles. This is
373 also supported by the identification of multiple targets in our Y2H screen.

374 Nevertheless, *At*PR-6 was identified across the three Y2H libraries suggesting it is
375 a major target of Hs2B11. PR-6 proteins were initially identified by their upregulation
376 during biotic or abiotic stresses [29] and are divided into 17 families based on their
377 function [38]. Members of the *At*PR-6 family are protease inhibitors, with a low molecular
378 mass varying from 8 to 20 kDa, that inhibit proteolytic activities from animals, fungal and
379 vegetal origins [29]. In Arabidopsis, six *AtPR-6* genes have been identified that encode
380 for serine protease inhibitors [38]. The *At*PR-6 protein identified in our screen (At2g38870)
381 encodes for a small (7.6 kDa) potato type I serine protease inhibitor, which has been
382 shown to inhibit the *in vitro* growth of *F. graminearum* through endogenous inhibitor
383 activity [39] and confers resistance to *B. cinerea* when overexpressed in Arabidopsis [30].
384 One other *At*PR-6 member, At5g43580 (Unusual Serine Protease Inhibitor; UPI), also
385 provides resistance against *B. cinerea* and a generalist herbivore *Trichoplusia ni* [40].
386 Here, we show that *At*PR-6 positively regulates flg22-mediated oxidative species
387 production, demonstrating a direct role in immune signaling, and provides resistance
388 against BCN infection. Several serine protease inhibitors in this family are also

389 upregulated in soybean in response to SCN infection [41], which could suggest a
390 conserved role in defense against parasitic nematodes.

391 In order to begin to dissect the role of *At*PR-6 in Arabidopsis we investigated its
392 spatio-temporal localization. GUS reporter-aided promoter analysis indicated that *AtPR-*
393 *6* is upregulated as an early response to BCN infection, which corresponds to the time
394 frame in which nematodes suppress defense and initiate the formation of the feeding site.
395 Using *pAtPR-6:GUS* reporter lines, we demonstrated that *AtPR-6* gene expression is
396 upregulated in syncytia at early stages of infection (4 dpi), but not at later stages (14 dpi).
397 These results are consistent with RNA-seq expression data of *At*PR-6 during infection
398 [25], with a peak of expression at 10 hpi. These results are also in line with the number
399 of captures of *At*PR-6 in the three different Y2H cDNA libraries using *Hs*2B11 as a bait
400 (11 captures at 3 dpi, 1 capture at 7 dpi and 3 captures at 10 dpi). It is possible that *At*PR-
401 6 could interact with secreted proteases to regulate host defense responses. Indeed,
402 RNA-seq analysis shows a number of effector serine proteases in BCN-infected
403 Arabidopsis during early infection [36]. *Hs*2B11 may have evolved to counteract *At*PR-6-
404 mediated protease inhibition, placing *Hs*2B11 and *At*PR-6 as players in the co-evolution
405 between BCN and their host.

406 The role of host- and pathogen-encoded serine protease inhibitors in effector-
407 triggered immunity (ETI) have been well-studied [42,43], however their involvement in
408 microbe-associated molecular pattern (MAMP)-triggered responses is not as well known.
409 Since *At*PR-6 has a role in regulating flg22-elicited ROS production in the absence of
410 nematode infection, we expect that it interacts with plant serine proteases in order to
411 execute endogenous functions. Indeed, our Y2H screen uncovered 22 plant candidate

412 *At*PR-6 interactors, among which we found three plant proteases predicted to be found in
413 the apoplast. The first protease is the subtilisin-like serine protease *At*SBT5.2, a serine
414 protease that attenuates the transcriptional activation of defense by the MYB30
415 transcription factor in Arabidopsis, therefore acting as a negative regulator of immunity
416 [44]. This gene also serves a direct role in attenuating defense by inactivating flagellin
417 immunogenicity through cleavage of the flg22 epitope [45]. Since *At*PR-6 interacts with
418 *At*SBT5.2, and possesses serine protease inhibitor activity, it is feasible that it could inhibit
419 *At*SBT5.2 activity as a means of promoting defense responses. The second plant
420 protease identified as a potential partner of *At*PR-6 is a subtilase family protein, also
421 belonging to a family of serine proteases [46]. We also found a eukaryotic aspartyl
422 protease as a potential interactor of *At*PR-6 which is S-nitrosylated in response to flg22
423 treatment in Arabidopsis [47], although a direct role in immunity has not been established.
424 We additionally captured three proteins from the nematode that interacted with *At*PR-6
425 during this screen, two of which are uncharacterized proteins carrying secretion signal
426 peptides, which would be interesting candidates for future investigations. Altogether, our
427 results indicate that *At*PR-6 could interact with endogenous plant proteases in order to
428 promote defense responses in Arabidopsis.

429 In order to gain structural insight into the interaction between *Hs*2B11 and *At*PR-
430 6, we modeled each of these proteins, individually, using *in silico* folding with AlphaFold2.
431 This is the first instance in which a 3D prediction software has successfully folded an
432 unknown domain in a phytoparasitic nematode effector with such high confidence,
433 emphasizing the need to predict the 3D structure of the entire effectorome in the future to
434 help researchers unravel effector functions. Structural predictions of *Hs*2B11 have

435 provided us clues about how it could interact with *At*PR-6. The intriguing structure of the
436 C-terminal domain of *Hs*2B11, with a tower-like structure that harbors an alignment of
437 serine on one edge, suggests that these serine residues could mimic the serine residue
438 present in the catalytic pocket of serine proteases. This could explain how two to four
439 repetitions alone are able to interact with *At*PR-6. There are two major mechanisms of
440 protease inhibition, irreversible interactions and tight reversible interactions [43]. In
441 irreversible interactions the protease cleaves the protease inhibitor in a way that destroys
442 the catalytic site of protease. As a consequence, the protease inhibitor is sacrificed at the
443 cost of the interactions. In contrast, reversible tight interactions occur by binding to the
444 active site in a substrate-like fashion. This latter type of interaction has been conclusively
445 demonstrated for serine protease inhibitors. We therefore can envision that the C-terminal
446 domain of *Hs*2B11 mimics the active site of a serine protease to temporarily sequester
447 *At*PR-6, titrating its activity as a positive immune regulator in order to favor BCN infection.
448 The involvement of these serine residues in the interaction will need to be further
449 investigated to better understand if and precisely how the effector *Hs*2B11
450 mechanistically traps *At*PR-6 to dampen plant basal immunity. This type of mechanism
451 has been demonstrated for the *Magnaporthe oryzae* effector AvrPiz-t that targets the
452 trypsin protease inhibitor APIP4 (AvrPiz-t interacting protein 4) and suppresses its activity
453 in order to promote infection [48]. Future work will need to investigate if *Hs*2B11 has a
454 direct effect on *At*PR-6 protease inhibitor activity or if the effector functions by limiting the
455 accumulation of free *At*PR-6 in a sequestering reaction.

456 In our experiments, we observed that *Hs*2B11 and *At*PR-6 are localized to the
457 cytoplasm and ER, and formed cytoplasmic punctuated structures resembling vesicles,

458 which could indicate that these proteins transit through the plant cell secretion pathway
459 to reach the apoplast. In our BiFC experiments, we also observed that *Hs*2B11 and *At*PR-
460 6 interact in the ER and the cytoplasm. At least two independent studies have shown that
461 the *At*PR-6 encoded by At2g38870 can be identified in the apoplast of Arabidopsis by
462 mass spectrometry [49,50]. Another *At*PR-6 protein, UPI, also accumulates in the
463 extracellular space, specifically in response to methyl jasmonic acid [30]. UPI is also
464 upregulated at 10 hpi with BCN (Fig S2), which could suggest that these proteins act
465 together in early defense against phytoparasitic nematodes. Nevertheless, we did not
466 observe expression of either *Hs*2B11 or *At*PR-6 in the apoplast under our conditions.
467 Future work is needed to determine where *Hs*2B11 localizes during natural infection and
468 whether *At*PR-6 is localized to the apoplast during BCN infection.

469 Together, our data indicate that *At*PR-6 is a defense protein upregulated in
470 response to BCN infection, possibly to inhibit the action of plant and/or nematode
471 proteases to prevent nematode infection. We hypothesize that *Hs*2B11 is secreted to
472 titrate *At*PR-6 in order to dampen its immune activity in the host during infection. This
473 work provides the first evidence of a cyst-nematode effector targeting a protease inhibitor
474 involved in host defense.

475

476 ## Materials and methods

477 ### Plasmid Construction

478 For 35S promoter-driven expression of *Hs*2B11 and *At*PR-6 expression lines, the coding
479 region of *Hs*2B11 (minus signal peptide) or *At*PR-6 was amplified from parasitic BCN

480 cDNA and Arabidopsis cDNA, respectively using gene-specific primers designed to
481 create the BamHI and SstI restriction sites, respectively (Table S2). All PCR
482 amplifications were performed using the Q5 DNA polymerase (New England Biolabs)
483 according to the manufacturer's instructions. The PCR products were digested, gel
484 purified, ligated into the binary vector pBI121, and verified by Sanger sequencing. For the
485 *At*PR-6 promoter construct, an 846 bp fragment upstream of the start codon of the *At*PR-
486 6 gene was amplified from Arabidopsis genomic DNA using forward and reverse primers
487 containing XbaI and BamHI restriction sites, respectively (Table S2). The purified PCR
488 product was digested by XbaI and BamHI, gel purified, cloned into XbaI-BamHI restriction
489 sites of binary vector pBI101, and confirmed by Sanger sequencing. For subcellular
490 localization or split-luciferase complementation assays, the full-length *Hs*2B11, or its
491 truncation variants, as well as the *At*PR-6 sequences, were amplified using gene specific
492 primers that contain the AttB1 and AttB2 recombination sites. A two-step PCR using AttB
493 adapter primer pairs was used to add the complete AttB recombination sites. The
494 sequences were recombined using the BP Clonase II into a pDONR221 vector and
495 verified by Sanger sequencing. For the subcellular localization, the corresponding
496 recombinant pDONR211 were used in a LR reaction along with the pK7WGF2,
497 pK7FWG2, pK7WGR2, pK7RWG2 destination vectors to produce the *Hs*2B11 and *At*PR-
498 6 fusions with GFP and RFP, respectively, in both orientations. For split-luciferase
499 complementation assays, the corresponding pDONR211 were used in a LR reaction
500 along with the pGWB-nLuc and pGWB-cLuc vectors to produce the *Hs*2B11 and *At*PR-6
501 fusions with the N- or C-terminal portion of the luciferase gene.

502

503 **Generation of Transgenic Arabidopsis Plants**

504 The *Agrobacterium tumefaciens* strain C58 was transformed with the binary plasmids by
505 the freeze-thaw method [51] and used to transform Arabidopsis Col-0 plants using the
506 floral dip method, as described previously by [52]. Transformed T1 plants were screened
507 on Murashige and Skoog (MS) medium containing kanamycin. and homozygous T3 were
508 used for subsequent analysis. The *AtPR-6* knockout line Salk_111051C was obtained
509 from the Salk Institute and homozygous plants were identified by genotyping.

510

511 **Plant Materials and Growth Conditions**

512 For ROS burst assays, RT-qPCR analysis and phenotyping, Arabidopsis plants
513 selected on MS plates containing kanamycin were transferred to Sunshine Mix #1-F1P
514 (Sun Gro Horticulture, Agawam, MA, USA) and fertilized with osmocote beads once every
515 two weeks. Plants were grown in a temperature-controlled growth chamber at 22 °C under
516 a 10-h light/14-h dark (150 to 160 μE · m2 · s−1) and no humidity control. For plate-based
517 assays, including BCN infection assays and root length measurements, seeds were
518 surface-disinfected with 70% (v/v) ethanol for 2 minutes, followed by sterilization in a 3%
519 (v/v) sodium hypochlorite solution (Clorox, California, USA) for 15 minutes. Seeds were
520 then rinsed several times with sterile distilled water to remove residual bleach. For the
521 nematode infection assay, sterilized seeds were germinated on modified Knop's medium
522 solidified with 0.8% (w/v) Daishin agar in 12-well tissue culture plates.

523 For root measurements, sterilized seeds were sown on square Petri dishes
524 containing half-strength Murashige and Skoog (1/2 MS) medium. To facilitate root growth

525 along the agar surface and allow for clear phenotypic observation, the plates were
526 maintained at a slight incline from the vertical. Root length was measured 21 days after
527 sowing. To ensure sufficient biological replication, 36 plates were utilized for each
528 genotype. *N. benthamiana* plants used for transient expression assays, BiFC and split-
529 luciferase complementation were grown in Sunshine Mix #1-F1P (Sun Gro Horticulture,
530 Agawam, MA, USA), and fertilised with osmocote beads once every two weeks. Plants
531 were under long-day conditions (16-h light/8-h dark) at 24°C.

532

533 **GUS Assays**

534 Monitoring of *AtPR6* gene expression was conducted on three-week old, *in vitro* grown
535 Arabidopsis *pAtPR-6:GUS* lines. For expression following BCN infection, plants were
536 inoculated with 250 BCN J2s and collected at 4 and 14 dpi. Histochemical detection of
537 GUS activity was performed according to [53] for 30 min or 4 hours at 37°C in the
538 presence of X-Gluc, as noted in the text.

539

540 **Nematode Infection Assays**

541 Ten-day-old seedlings were inoculated with approximately 250 surface-sterilized J2 *H.*
542 *schachtii* nematodes per plant, as described previously [54]. The inoculated plants were
543 maintained under the same conditions described above for an additional 3 weeks before
544 counting the J4 adult females. Mean values significantly different from that of the wild type
545 were determined in a modified T-test using the statistical software package SAS ($P<0.05$).
546 Two independent biological replicates were established for each set of conditions.

547 **RNA extraction and RT-qPCR analysis**

548 Approximately 50 mg of 3-week-old Arabidopsis tissue was used for total RNA isolation
549 using TRIzol reagent (Invitrogen) according to the manufacturer's instructions. Two µg of
550 RNA and the Maxima First Strand cDNA Synthesis kit with dsDNase (ThermoFisher) were
551 used for cDNA synthesis. A quantitative real-time PCR assay was performed on a 7500
552 real-time PCR system (Applied Biosystems, CA, USA) using iTaq Universal SYBR Green
553 Supermix (BioRad). For assessment of the overexpression of *Hs2B11* or *AtPR-6*,
554 *AtUBOX* (AT5G15400) was chosen as an internal control to normalize the data. The
555 transcript level was calculated using the $2^{-\Delta\Delta CT}$ method [55]. Primers used for RT-qPCR
556 analysis can be found in Table S2.

557

558 **Yeast Two-Hybrid Assays**

559 Y2H screening was performed as described in the BD Matchmaker Library Construction
560 and Screening Kits user manual (Clontech). The coding sequence of *Hs*2B11 o*r At*PR-6
561 was amplified using forward and reverse primers containing EcoRI and BamHI restriction
562 sites, respectively (Table S2), and fused to the GAL4 DNA-binding domain of pGBKT7
563 vector to generate pGBKT7-*Hs*2B11 and then introduced into the *Saccharomyces*
564 *cerevisiae* strain Y187 to generate bait strains. Three Arabidopsis cDNA libraries from
565 roots of ecotype C24 at 3, 7, and 10 dpi after *H. schachtii* infection were generated in *S.*
566 *cerevisiae* strain AH109 as a fusion to the GAL4 activation domain of pGADT7-Rec2
567 vector [56]. Screening for interacting proteins and subsequent analyses were performed
568 as described by Clontech protocols with one Y2H screen with each library for *Hs*2B11,

569 and one Y2H screen using a pool of the three libraries for *At*PR-6 bait. To test the potential
570 interaction between full-length or truncated version of *Hs*2B11 and *At*PR-6, the coding
571 sequence of *Hs*2B11 (full-length or truncated) or AtPR-6 was amplified using forward and
572 reverse primers containing EcoRI and BamH1 restriction sites, respectively (Table S2),
573 and fused to the GAL4 DNA activation domain of pGADT7 prey vector to generate
574 pGADT7 recombinant vectors, then introduced into *S. cerevisiae* strain AH109 in
575 combination with the bait vector containing *Hs*2B11 sequences or human Lamin C. The
576 pairwise interaction was tested following Clontech protocols.

577

578 **Bimolecular Fluorescence Complementation Assays**

579 The pDOE vectors series have been used to perform the BiFC experiment [57]. The full-
580 length coding sequence of *Hs*2B11 or its C-terminal domain was amplified using specific
581 primers containing NcoI and SpeI. The coding sequence of *At*PR-6 was amplified with
582 specific primers containing KflI and BspEI. The *Hs*2B11 amplicons were digested and
583 cloned into pDOE105, pDOE106, pDOE107 and pDOE108. Subsequently, *At*PR-6
584 amplicons were digested and cloned into the vectors already containing the *Hs*2B11 full-
585 length or C-terminus domain sequences, or empty vectors to produce the BiFC vectors.
586 Those vectors were transformed into *A. tumefaciens* GV3101 strain through freeze-thaw
587 method. The presence of the insert and vectors were confirmed by colony PCR.

588

589

590

591 **Transient protein expression and confocal microscopy**

592 Transient expression was achieved by infiltrating *N. benthamiana* leaves
593 with *A. tumefaciens* GV3101 strains harboring GFP- or RFP-fusion or BiFC constructs at
594 a OD (600 nm) between 0.5 and 1, as described previously (REF). Leaves were imaged
595 48 h after agroinfiltration, with a confocal microscope (LSM700) equipped with an Argon
596 ion and HeNe laser as the excitation source. For simultaneous GFP/RFP imaging,
597 samples were excited at 488 nm for GFP and 551 nm for mRFP, in the multi-track
598 scanning mode. For simultaneous YFP/CFP imaging, samples were excited at 488 nm
599 for GFP and 405 nm for CFP, in the multi-track scanning mode. GFP or YFP emission
600 was detected selectively with a 505–530 nm band-pass emission filter. CFP emission was
601 detected selectively with a 460-500 nm band-pass emission filter. We detected mRFP
602 fluorescence with a 560–615 nm band-pass emission filter. The ER marker pCMU-
603 AtWak2-mCherry-HDEL [58] was used for co-localization studies.

604

605 **Split-luciferase complementation assays**

606 Transient expression was achieved by infiltrating *N. benthamiana* leaves
607 with *A. tumefaciens* GV3101 strains harboring split-luciferase constructs at O.D (600 nm)
608 0.3 each. Three days after infiltration, six discs per construction were collected and
609 incubated with 1 mM luciferin for 15 min in the dark in a 96 well-plate, before reading the
610 luminescence using the SpectraMax spectrophotometer.

611

612

613 **Oxidative Burst Assays**

614 Flg22- elicited ROS production was measured in 4–5-week-old Arabidopsis plants grown
615 on soil and conducted as described previously [59]. Briefly, six leaf discs, per genotype,
616 were collected in a 96-well plate containing 100 µL of water and incubated overnight in
617 the dark at room temperature. The next day water was replaced with a solution containing
618 100 µM luminol, 10 µg/mL HRP, and 100 nM of flg22 peptide. Readings were taken using
619 a LUM96 module every 2 min over 40 min, with a 1000 ms integration time.

620

621 ## Author Contributions

622 JM, PJ, MB and TJB conceived and designed the experiments. JM, MB, AK, PJ, TM and
623 EK performed the experiments. JM, PJ, MB and TJB analyzed the data. JM, MB and TJB
624 wrote the article with input from all authors. TJB and SAW supervised the work. TJB
625 provided funding for the work.

626

627 ## Acknowledgments

628 We thank Jackson Goshon for technical assistance.

629

630 ## Funding and Conflicts of Interest

631 This project was funded by the North Central Soybean Research Program (NCSRP) and
632 by the Iowa Agriculture and Home Economics Experiment Station, Ames, IA, supported
633 by Hatch Act and State of Iowa funds.

634 ## References

635 1. Dilawari R, Kaur N, Priyadarshi N, Prakash I, Patra A, Mehta S, et al. Soybean: A key
636 player for global food security. Soybean Improvement. Cham: Springer International
637 Publishing; 2022. pp. 1–46.

638 2. Rongli, Chen H, Yang Z, Yuan S, Zhou X ’an. Research status of soybean symbiosis
639 nitrogen fixation. Oil Crop Science. 2020;5: 6–10.

640 3. Phani V, Khan MR, Dutta TK. Plant-parasitic nematodes as a potential threat to protected
641 agriculture: Current status and management options. Crop Prot. 2021;144: 105573.

642 4. Mitchum MG, Hussey RS, Baum TJ, Wang X, Elling AA, Wubben M, et al. Nematode
643 effector proteins: an emerging paradigm of parasitism. New Phytol. 2013;199: 879–894.

644 5. Triffitt MJ. Observations on the life-cycle of Heterodera schachtii. J Helminthol. 1930;8:
645 185–196.

646 6. Gupta R, Mfarrej MFB, Elnour RO, Hashem M, Ahmad F. Defence response of host plants
647 for cyst nematode: A review on parasitism and defence. J King Saud Univ Sci. 2023;35:
648 102829.

649 7. Hewezi T, Baum TJ. Manipulation of plant cells by cyst and root-knot nematode effectors.
650 Mol Plant Microbe Interact. 2013;26: 9–16.

651 8. Wang Y, Wang Y, Wang Y. Apoplastic Proteases: Powerful Weapons against Pathogen
652 Infection in Plants. Plant Commun. 2020;1: 100085.

653 9. Figaj D, Ambroziak P, Przepiora T, Skorko-Glonek J. The Role of Proteases in the
654 Virulence of Plant Pathogenic Bacteria. Int J Mol Sci. 2019;20. doi:10.3390/ijms20030672

655 10. Chandrasekaran M, Thangavelu B, Chun SC, Sathiyabama M. Proteases from
656 phytopathogenic fungi and their importance in phytopathogenicity. J Gen Plant Pathol.
657 2016;82: 233–239.

658 11. Vieira P, Danchin EGJ, Neveu C, Crozat C, Jaubert S, Hussey RS, et al. The plant
659 apoplasm is an important recipient compartment for nematode secreted proteins. J Exp
660 Bot. 2011;62: 1241–1253.

661 12. Zhang J, Li W, Xiang T, Liu Z, Laluk K, Ding X, et al. Receptor-like cytoplasmic kinases
662 integrate signaling from multiple plant immune receptors and are targeted by a
663 Pseudomonas syringae effector. Cell Host Microbe. 2010;7: 290–301.

664 13. Qi D, Dubiella U, Kim SH, Sloss DI, Dowen RH, Dixon JE, et al. Recognition of the protein
665 kinase AVRPPHB SUSCEPTIBLE1 by the disease resistance protein RESISTANCE TO
666 PSEUDOMONAS SYRINGAE5 is dependent on s-acylation and an exposed loop in
667 AVRPPHB SUSCEPTIBLE1. Plant Physiol. 2014;164: 340–351.

668 14. Bellafiore S, Shen Z, Rosso M-N, Abad P, Shih P, Briggs SP. Direct identification of the
669 Meloidogyne incognita secretome reveals proteins with host cell reprogramming potential.
670 PLoS Pathog. 2008;4: e1000192.

671 15. Hu L-J, Wu X-Q, Ding X-L, Ye J-R. Comparative transcriptomic analysis of candidate
672 effectors to explore the infection and survival strategy of Bursaphelenchus xylophilus during
673 different interaction stages with pine trees. BMC Plant Biol. 2021;21: 224.

674 16. Haegeman A, Mantelin S, Jones JT, Gheysen G. Functional roles of effectors of plant-
675 parasitic nematodes. Gene. 2012;492: 19–31.

676 17. Margets A, Foster J, Kumar A, Maier TR, Masonbrink R, Mejias J, et al. The Soybean Cyst

677 Nematode Effector Cysteine Protease 1 (CPR1) Targets a Mitochondrial Soybean
678 Branched-Chain Amino Acid Aminotransferase (GmBCAT1). Mol Plant Microbe Interact.
679 2024;37: 751–764.

680 18. Pekkarinen AI, Longstaff C, Jones BL. Kinetics of the inhibition of fusarium serine
681 proteinases by barley (Hordeum vulgare L.) inhibitors. J Agric Food Chem. 2007;55: 2736–
682 2742.

683 19. A Bowman–Birk-Type Trypsin-Chymotrypsin Inhibitor from Broad Beans. Biochem Biophys
684 Res Commun. 2001;289: 91–96.

685 20. Liu Y, Gong T, Kong X, Sun J, Liu L. XYLEM CYSTEINE PEPTIDASE 1 and its inhibitor
686 CYSTATIN 6 regulate pattern-triggered immunity by modulating the stability of the NADPH
687 oxidase RBOHD. Plant Cell. 2023; koad262.

688 21. Song J, Win J, Tian M, Schornack S, Kaschani F, Ilyas M, et al. Apoplastic effectors
689 secreted by two unrelated eukaryotic plant pathogens target the tomato defense protease
690 Rcr3. Proc Natl Acad Sci U S A. 2009;106: 1654–1659.

691 22. Lozano-Torres JL, Wilbers RHP, Warmerdam S, Finkers-Tomczak A, Diaz-Granados A,
692 van Schaik CC, et al. Apoplastic venom allergen-like proteins of cyst nematodes modulate
693 the activation of basal plant innate immunity by cell surface receptors. PLoS Pathog.
694 2014;10: e1004569.

695 23. Pogorelko GV, Juvale PS, Rutter WB, Hütten M, Maier TR, Hewezi T, et al. Re-targeting of
696 a plant defense protease by a cyst nematode effector. Plant J. 2019;98: 1000–1014.

697 24. Noon JB, Hewezi T, Maier TR, Simmons C, Wei J-Z, Wu G, et al. Eighteen New Candidate
698 Effectors of the Phytonematode Heterodera glycines Produced Specifically in the Secretory

699 Esophageal Gland Cells During Parasitism. Phytopathology. 2015;105: 1362–1372.

700 25. Siddique S, Radakovic ZS, Hiltl C, Pellegrin C, Baum TJ, Beasley H, et al. The genome and
701 lifestage-specific transcriptomes of a plant-parasitic nematode and its host reveal
702 susceptibility genes involved in trans-kingdom synthesis of vitamin B5. Nat Commun.
703 2022;13: 6190.

704 26. Molloy B, Shin DS, Long J, Pellegrin C, Senatori B, Vieira P, et al. The origin, deployment,
705 and evolution of a plant-parasitic nematode effectorome. PLoS Pathog. 2024;20:
706 e1012395.

707 27. Jumper J, Evans R, Pritzel A, Green T, Figurnov M, Ronneberger O, et al. Highly accurate
708 protein structure prediction with AlphaFold. Nature. 2021;596: 583–589.

709 28. van Kempen M, Kim SS, Tumescheit C, Mirdita M, Lee J, Gilchrist CLM, et al. Fast and
710 accurate protein structure search with Foldseek. Nat Biotechnol. 2023. doi:10.1038/s41587-
711 023-01773-0

712 29. Sels J, Mathys J, De Coninck BMA, Cammue BPA, De Bolle MFC. Plant pathogenesis-
713 related (PR) proteins: a focus on PR peptides. Plant Physiol Biochem. 2008;46: 941–950.

714 30. Chassot C, Nawrath C, Métraux J-P. Cuticular defects lead to full immunity to a major plant
715 pathogen. Plant J. 2007;49: 972–980.

716 31. Alkharouf NW, Klink VP, Chouikha IB, Beard HS, MacDonald MH, Meyer S, et al.
717 Timecourse microarray analyses reveal global changes in gene expression of susceptible
718 Glycine max (soybean) roots during infection by Heterodera glycines (soybean cyst
719 nematode). Planta. 2006;224: 838–852.

720 32. Igarashi D, Bethke G, Xu Y, Tsuda K, Glazebrook J, Katagiri F. Pattern-triggered immunity

721 suppresses programmed cell death triggered by fumonisin b1. PLoS One. 2013;8: e60769.

722 33. Chiu T, Poucet T, Li Y. The potential of plant proteins as antifungal agents for agricultural
723 applications. Synth Syst Biotechnol. 2022;7: 1075–1083.

724 34. Dunaevskiĭ IE, Tsybina TA, Beliakova GA, Domash VI, Shapno TP, Zabreĭko SA, et al.
725 [Proteinase inhibitors as antistress proteins in higher plants]. Prikl Biokhim Mikrobiol.
726 2005;41: 392–396.

727 35. Liz MA, Faro CJ, Saraiva MJ, Sousa MM. Transthyretin, a new cryptic protease. J Biol
728 Chem. 2004;279: 21431–21438.

729 36. Siddique S, Coomer A, Baum T, Williamson VM. Recognition and Response in Plant-
730 Nematode Interactions. Annu Rev Phytopathol. 2022;60: 143–162.

731 37. Vijayapalani P, Hewezi T, Pontvianne F, Baum TJ. An Effector from the Cyst Nematode
732 Derepresses Host rRNA Genes by Altering Histone Acetylation. Plant Cell. 2018;30: 2795–
733 2812.

734 38. Ali S, Ganai BA, Kamili AN, Bhat AA, Mir ZA, Bhat JA, et al. Pathogenesis-related proteins
735 and peptides as promising tools for engineering plants with multiple stress tolerance.
736 Microbiol Res. 2018;212-213: 29–37.

737 39. Bleackley MR, Dawson CS, McKenna JA, Quimbar P, Hayes BME, van der Weerden NL, et
738 al. Synergistic Activity between Two Antifungal Proteins, the Plant Defensin NaD1 and the
739 Bovine Pancreatic Trypsin Inhibitor. mSphere. 2017;2. doi:10.1128/mSphere.00390-17

740 40. Laluk K, Mengiste T. The Arabidopsis extracellular UNUSUAL SERINE PROTEASE
741 INHIBITOR functions in resistance to necrotrophic fungi and insect herbivory. Plant J.
742 2011;68: 480–494.

743 41. Khan R, Alkharouf N, Beard H, Macdonald M, Chouikha I, Meyer S, et al. Microarray
744 analysis of gene expression in soybean roots susceptible to the soybean cyst nematode
745 two days post invasion. J Nematol. 2004;36: 241–248.

746 42. Jashni MK, Mehrabi R, Collemare J, Mesarich CH, de Wit PJGM. The battle in the
747 apoplast: further insights into the roles of proteases and their inhibitors in plant-pathogen
748 interactions. Front Plant Sci. 2015;6: 584.

749 43. Clemente M, Corigliano MG, Pariani SA, Sánchez-López EF, Sander VA, Ramos-Duarte
750 VA. Plant Serine Protease Inhibitors: Biotechnology Application in Agriculture and
751 Molecular Farming. Int J Mol Sci. 2019;20. doi:10.3390/ijms20061345

752 44. Serrano I, Buscaill P, Audran C, Pouzet C, Jauneau A, Rivas S. A non canonical subtilase
753 attenuates the transcriptional activation of defence responses in Arabidopsis thaliana. Elife.
754 2016;5. doi:10.7554/eLife.19755

755 45. Buscaill P, Sanguankiattichai N, Kaschani F, Huang J, Mooney BC, Li Y, et al. Subtilase
756 SBT5.2 inactivates flagellin immunogenicity in the plant apoplast. Nat Commun. 2024;15:
757 10431.

758 46. Schaller A, Stintzi A, Rivas S, Serrano I, Chichkova NV, Vartapetian AB, et al. From
759 structure to function - a family portrait of plant subtilases. New Phytol. 2018;218: 901–915.

760 47. Lawrence SR 2nd, Gaitens M, Guan Q, Dufresne C, Chen S. S-Nitroso-Proteome Revealed
761 in Stomatal Guard Cell Response to Flg22. Int J Mol Sci. 2020;21.
762 doi:10.3390/ijms21051688

763 48. Zhang C, Fang H, Shi X, He F, Wang R, Fan J, et al. A fungal effector and a rice NLR
764 protein have antagonistic effects on a Bowman-Birk trypsin inhibitor. Plant Biotechnol J.

765 2020;18: 2354–2363.

766 49. Boudart G, Jamet E, Rossignol M, Lafitte C, Borderies G, Jauneau A, et al. Cell wall
767 proteins in apoplastic fluids of Arabidopsis thaliana rosettes: identification by mass
768 spectrometry and bioinformatics. Proteomics. 2005;5: 212–221.

769 50. Jiang S, Pan L, Zhou Q, Xu W, He F, Zhang L, et al. Analysis of the apoplast fluid proteome
770 during the induction of systemic acquired resistance in Arabidopsis thaliana. PeerJ.
771 2023;11: e16324.

772 51. Höfgen R, Willmitzer L. Storage of competent cells for Agrobacterium transformation.
773 Nucleic Acids Res. 1988;16: 9877.

774 52. Clough SJ, Bent AF. Floral dip: a simplified method for Agrobacterium-mediated
775 transformation of Arabidopsis thaliana. Plant J. 1998;16: 735–743.

776 53. Jefferson RA, Kavanagh TA, Bevan MW. GUS fusions: beta-glucuronidase as a sensitive
777 and versatile gene fusion marker in higher plants. EMBO J. 1987;6: 3901–3907.

778 54. Baum TJ, Wubben MJ, Hardyy KA, Su H, Rodermel SR. A Screen for Arabidopsis thaliana
779 Mutants with Altered Susceptibility to Heterodera schachtii. J Nematol. 2000;32: 166–173.

780 55. Livak KJ, Schmittgen TD. Analysis of relative gene expression data using real-time
781 quantitative PCR and the 2(-Delta Delta C(T)) Method. Methods. 2001;25: 402–408.

782 56. Hewezi T, Howe P, Maier TR, Hussey RS, Mitchum MG, Davis EL, et al. Cellulose binding
783 protein from the parasitic nematode Heterodera schachtii interacts with Arabidopsis pectin
784 methylesterase: cooperative cell wall modification during parasitism. Plant Cell. 2008;20:
785 3080–3093.

786 57. Gookin TE, Assmann SM. Significant reduction of BiFC non-specific assembly facilitates in
787 planta assessment of heterotrimeric G-protein interactors. Plant J. 2014;80: 553–567.

788 58. Ivanov S, Harrison MJ. A set of fluorescent protein-based markers expressed from
789 constitutive and arbuscular mycorrhiza-inducible promoters to label organelles, membranes
790 and cytoskeletal elements in Medicago truncatula. Plant J. 2014;80: 1151–1163.

791 59. Bredow M, Sementchoukova I, Siegel K, Monaghan J. Pattern-Triggered Oxidative Burst
792 and Seedling Growth Inhibition Assays in Arabidopsis thaliana. JoVE (Journal of Visualized
793 Experiments). 2019; e59437.

794 60. Chicowski AS, Qi M, Variz H, Bredow M, Montes-Serey C, Caiazza F, et al. A soybean rust
795 effector protease suppresses host immunity and cleaves a 3-deoxy-7-phosphoheptulonate
796 synthase. bioRxiv. 2023. doi:10.1101/2023.09.07.556260

797

798

799

800

801

802

803

804

805

806

Figures and Legends

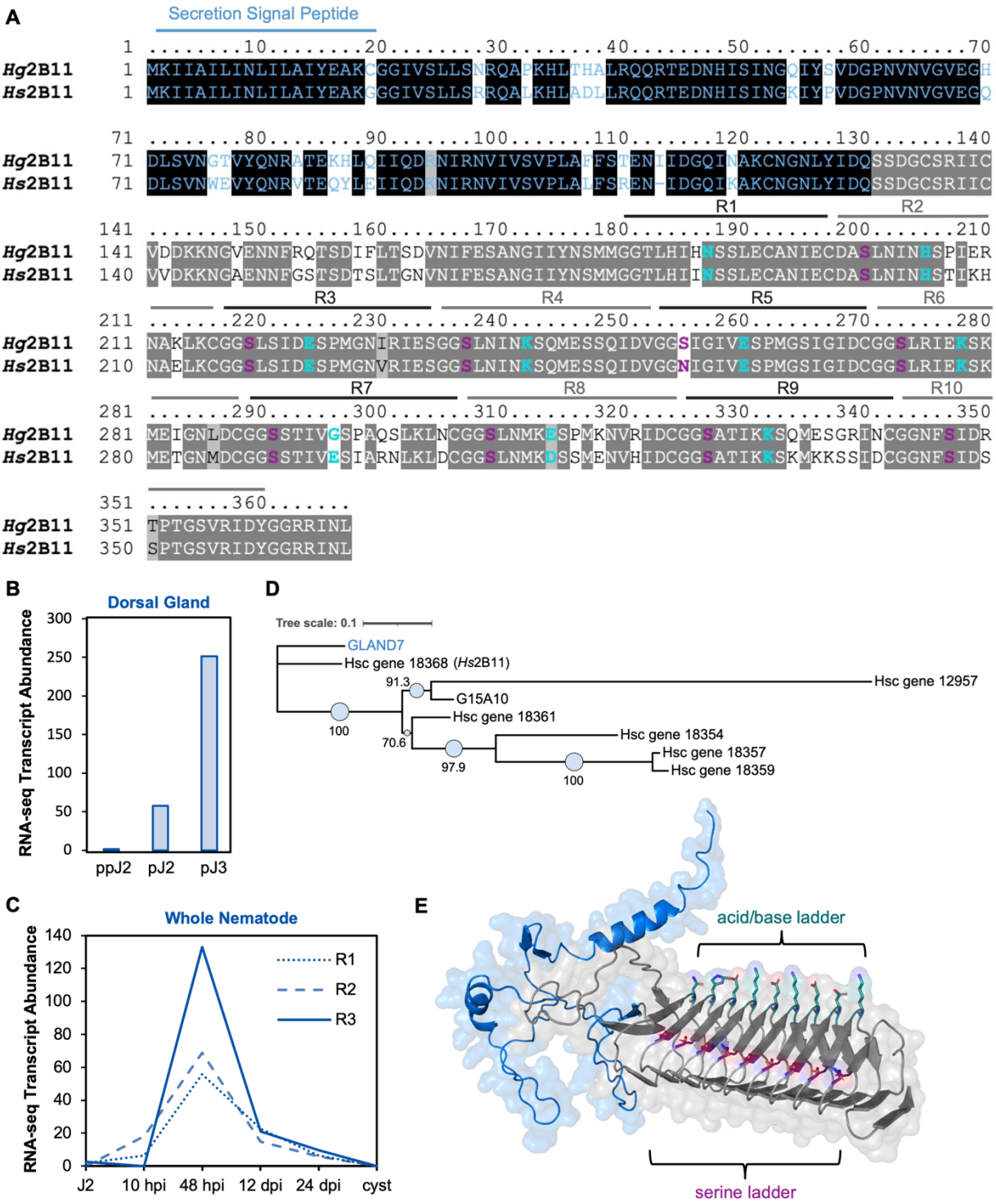

811 **Fig 1. *Hs*2B11 is a predicted effector protein expressed during early infection.** (A) Amino
812 acid sequence alignment of 2B11 effectors from *Heterodera glycines* and *Heterodera schachtii*
813 (*Hg*2B11 and *Hs*2B11). The N-terminal domain is indicated in blue text with conserved amino
814 acids in black boxes and the C-terminal domain is identified by black text with conserved residues
815 in gray boxes. The secretion signal peptide (SP) is indicated by a blue line and alternance of
816 repeats (R1-10) in the C-terminal domain are indicated by grey lines. Residues forming acid/base
817 and serine ladders are indicated in turquoise and purple, respectively. (B) RNA-seq expression
818 data from [26] showing the dorsal gland expression of *Hs*2B11 in pre-parasitic J2 (ppJ2), parasitic
819 J2 (pJ2) and parasitic J3 (pJ3) nematodes. (C) RNA-seq expression data from [25] showing the
820 expression of *Hs*2B11 (Hsc_gene_18368) during the life cycle of whole *H. schachtii* nematodes.
821 (D) Phylogenetic tree of the *H. schachtii* and *H. glycines* 2B11 family. The tree scale corresponds
822 to the number of substitutions per site based on the amino-acid matrix (JTT). The genes starting
823 with Hsc_ correspond to *H. schachtii* genes whereas GLAND7 and G15A10 belong to *H. glycines*.
824 (E) 3D structure of *Hs*2B11 as predicted by Alphafold2
825 (https://github.com/sokrypton/ColabDesign). The N-terminus is indicated in blue and the C-
826 terminus in grey. The alignment of serines or the alternance of acid and basic amino acids are
827 displayed in purple and turquoise, respectively.
828
829
830
831
832
833
834

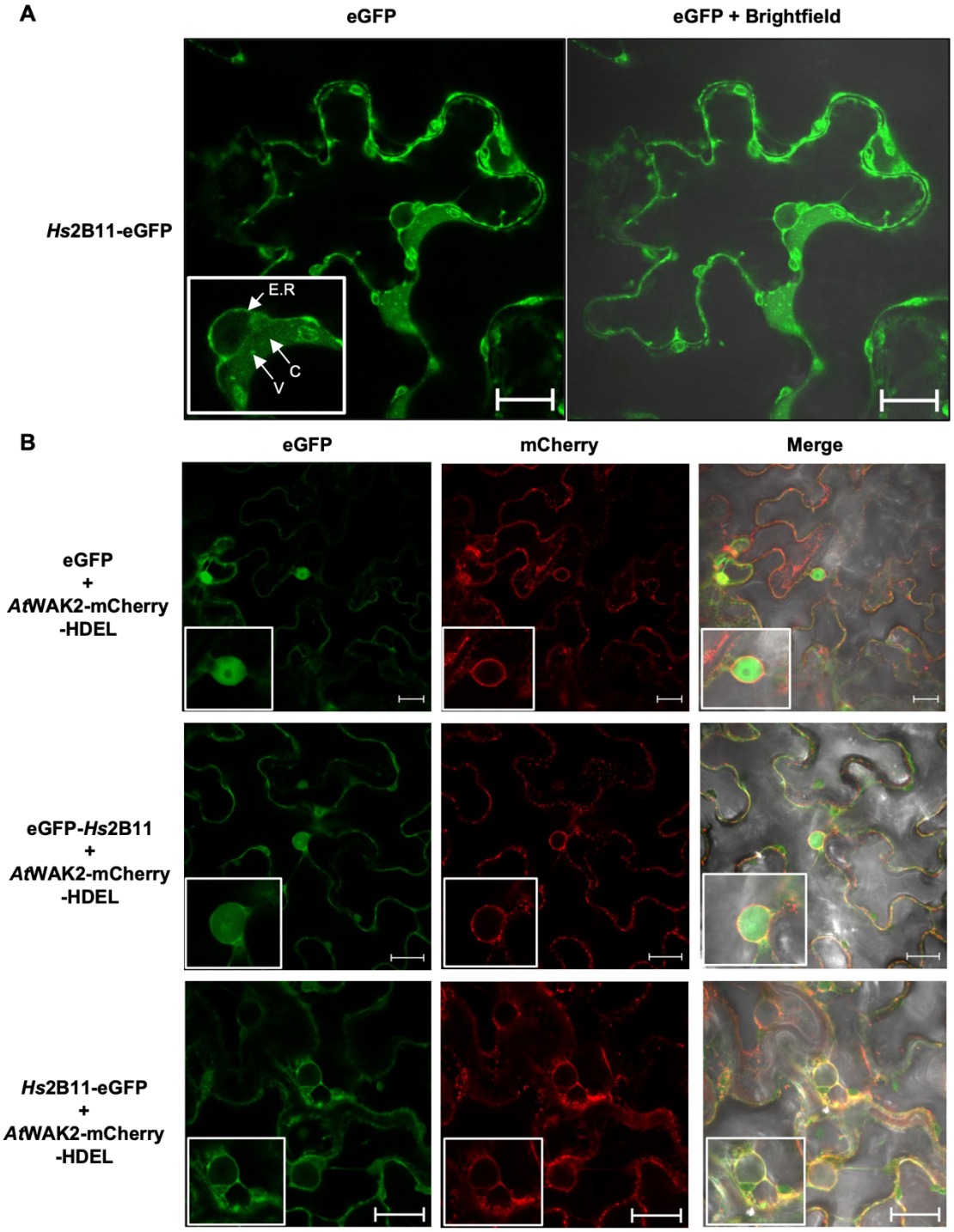

835

836

837 **Fig 2. *Hs*2B11 localizes to the cytoplasm and endoplasmic reticulum in *Nicotiana***

838 ***benthamiana.*** (A) Subcellular localisation of transiently expressed *Hs*2B11-eGFP in *N.*

839 *benthamiana* leaves 2 dpi. (B) Co-localization of eGFP-*Hs*2B11 and *Hs*2B11-eGFP with the *A.*
840 *thaliana* endoplasmic reticulum marker *At*WAK2-mCherry-HDEL. E.R= endoplasmic reticulum;
841 C= cytoplasm; V= vesicle. Experiments were conducted two times with similar results. Bar = 20
842 μM.
843
844
845
846
847
848
849
850
851
852
853
854
855
856
857

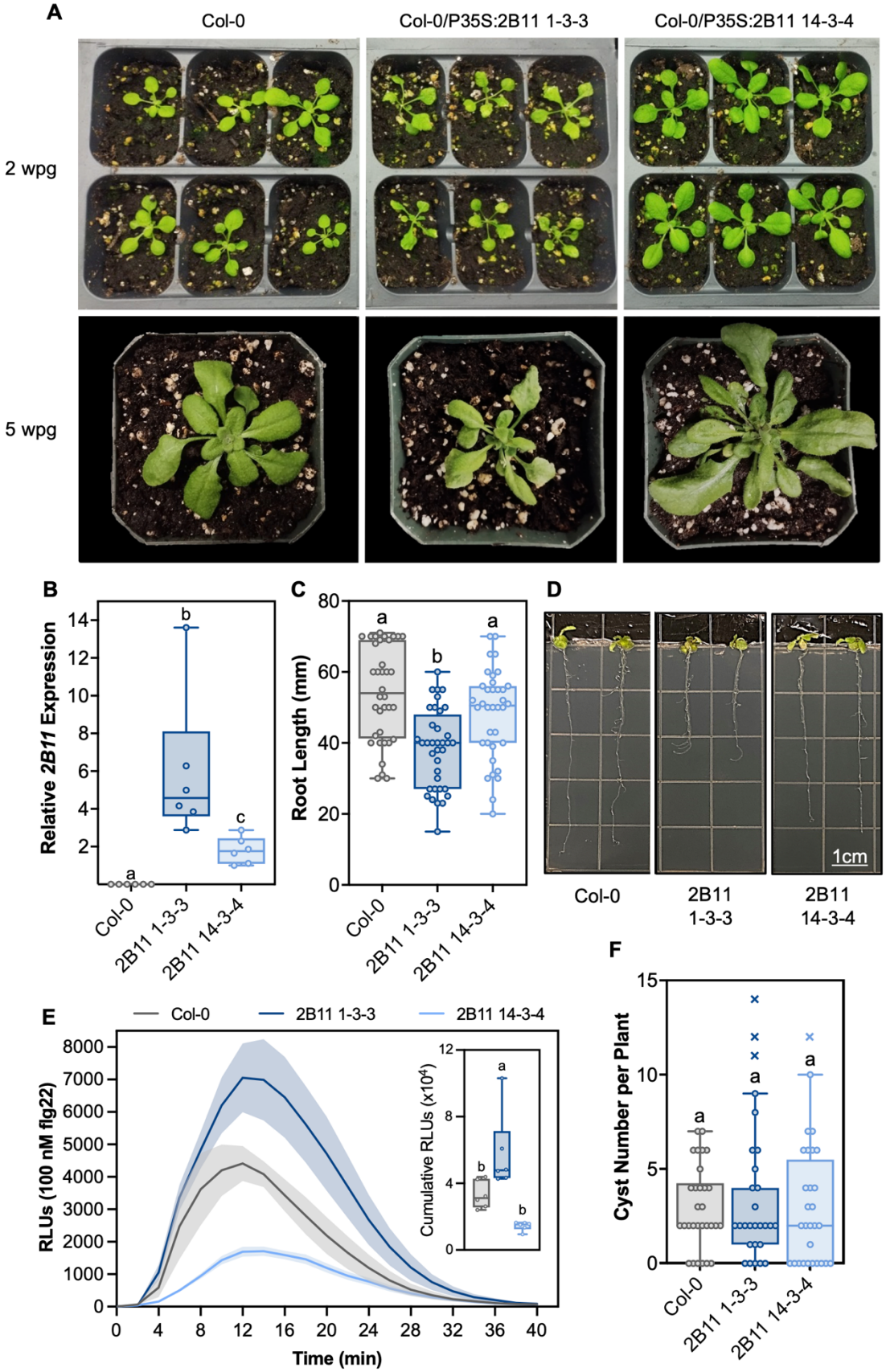
A
Col-0
Col-0/P35S:2B11 1-3-3
Col-0/P35S:2B11 14-3-4
2 wpg
5 wpg
B
Relative 2B11 Expression
Col-0
2B11 1-3-3
2B11 14-3-4
C
Root Length (mm)
D
1cm
E
Col-0
2B11 1-3-3
2B11 14-3-4
RLUs (100 nM flg22)
Time (min)
Cumulative RLUs (x10⁴)
F
Cyst Number per Plant

858

859 **Fig 3. *Hs*2B11 expression in Arabidopsis leads to contrasting growth and immune**
860 **phenotypes.** (A) Photos of two independent transgenic Arabidopsis lines expressing *Hs*2B11 at
861 2 and 5 weeks post germination (2 wpg and 5 wpg), compared to non-transgenic Columbia (Col-
862 0) controls. (B) Expression levels of *Hs2B11* in transgenic lines assessed by RT-qPCR.
863 Transcripts were normalized to the Arabidopsis housekeeping gene *qUBOX* and compared to
864 Col-0 control plants. (C-D) Root growth of *Hs2B11* expression lines on MS media. (E) Flg22-
865 elicited oxidative species production in *Hs2B11* expressing lines compared to Col-0 controls over
866 a 40 min time course represented as a dynamic curve and cumulative relative light units. (F)
867 Number of cysts per plant in wild-type Col-0 and two *Hs2B11*-expressing lines. Results from two
868 independent experiments are pooled. “x” symbols represent outliers identified using a Grubb’s
869 test. Box plots display interquartile range (25th to 75th percentile) split by a mean line. Whiskers
870 represent maximum and minimum values. Statistically significant values ($p<0.05$) are indicated
871 by different lower case letters as determined by a one-way analysis of variance followed by
872 Tukey's post-hoc test. Unless indicated, representative data from one of two experiments is
873 shown.
874
875
876
877
878
879
880
881
882
883

A

	Number of capture	Loci	Gene Annotation
3 dpi Library	**11**	**AT2G38870**	**PR-6 proteinase inhibitor family**
	2	AT3G14240	Subtilase family protein
	2	AT5G51970	Putative sorbitol dehydrogenase
	1	17 other proteins	
7 dpi Library	**Number of capture**	**Loci**	**Gene Annotation**
	2	AT2G20990	SYNAPTOTAGMIN A, ATSYT1
	2	AT1G60680	NAD(P)-linked oxidoreductase superfamily protein
	1	**AT2G38870**	**PR-6 proteinase inhibitor family**
	1	14 other proteins	
10 dpi Library	**Number of capture**	**Loci**	**Gene Annotation**
	3	**AT2G38870**	**PR-6 proteinase inhibitor family**
	3	ATMG00020	mitochondrial 26S ribosomal RNA protein
	2	AT3G45760	Nucleotidyltransferase family protein
	1	32 other proteins	

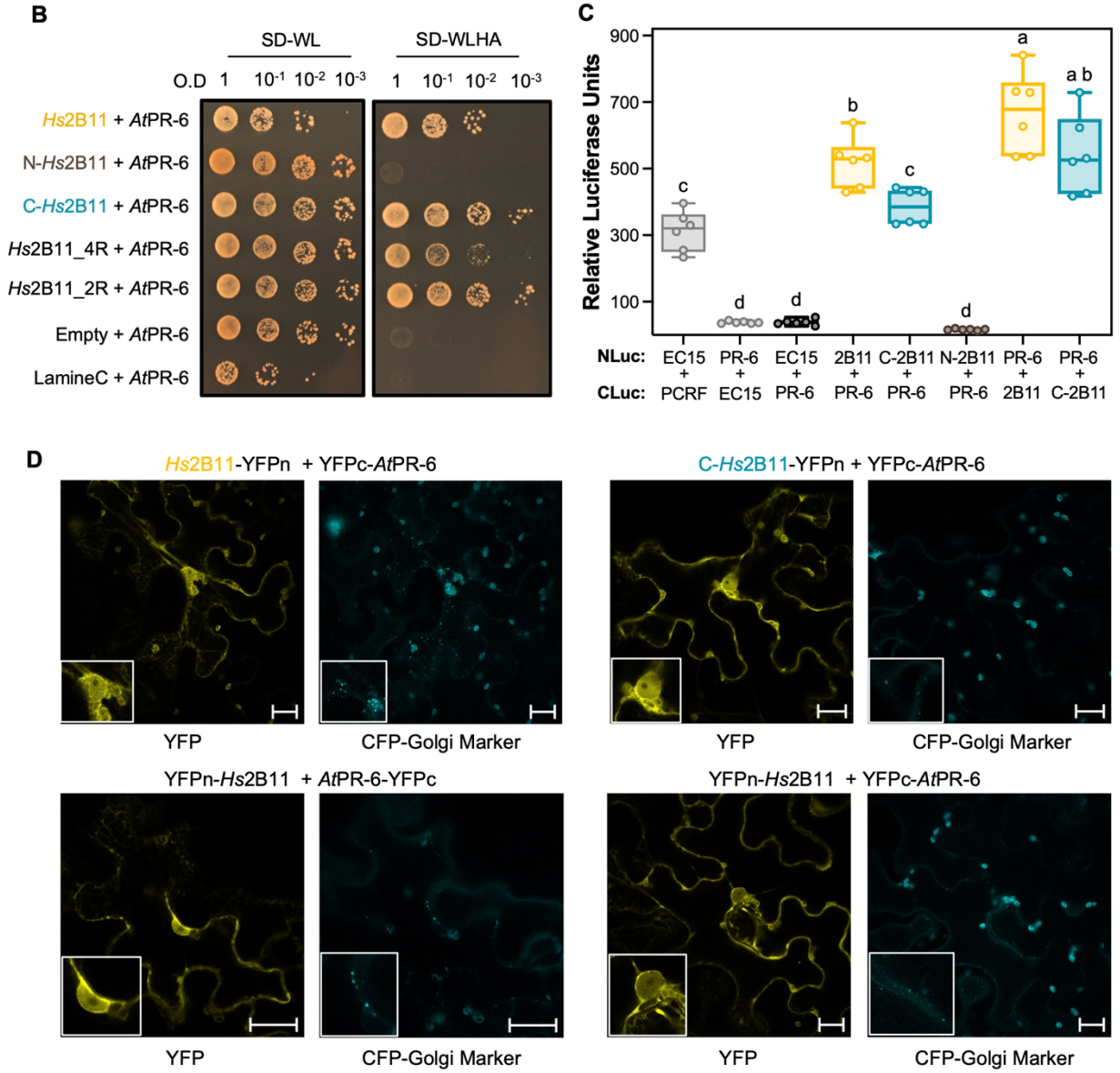

884

885 **Fig 4. *Hs*2B11 interacts with *At*PR-6 in yeast and *in planta*.** (A) Summary of the three
886 independent Y2H screen results against the three libraries of Arabidopsis infected with BCN at 3,
887 7 and 10 dpi, using *Hs*2B11 as a bait. The number of captures corresponds to the same gene
888 found in independent yeast colonies. (B) Pair-wise Y2H validation of the protein-protein interaction
889 between *Hs*2B11 and *At*PR-6. The N- and C-terminal domains of *Hs*2B11 correspond to the
890 amino acid sequences identified in Fig 1A. *Hs*2B11_2R and *Hs*2B11_4R are composed of 2 or 4
891 loops of the C-terminal domain of *Hs*2B11. Yeast carrying both vectors (pGBK-T7 and pGAD-T7)
892 are selected on SD-WL media whereas yeast carrying a protein-protein interaction are selected
893 on SD-WLHA, LamineC is used as a negative control. (C) Split-luciferase complementation assay
894 in *N. benthamiana* leaves. The *Phakospora pachyrhizi* effector *Pp*EC15 and its interacting host
895 target, PCRF [60], were used as positive control and *Pp*EC15 with *At*PR-6 was used as a negative
896 control. Lower case letters represent statistically significant groups ($p<0.05$) determined using a
897 one-way analysis of variance followed by a post-hoc Tukey test. Box plots display interquartile
898 range (25th to 75th percentile) split by a mean line. Whiskers represent maximum and minimum
899 values. Experiments were conducted twice with similar results. (D) BiFC analysis of *Hs*2B11 and
900 *At*PR-6 indicate that the proteins interact in the cytoplasm and endoplasmic reticulum of *N.*
901 *benthamiana* epidermal cells. Yellow fluorescent protein (YFP) confocal images of BiFC
902 experiments with different combinations of YFPc or YFPn fused, at the C- or N-terminus, to
903 *Hs*2B11 and *At*PR-6, expressed in *N. benthamiana* epidermal cells is shown on the left; and Cyan
904 fluorescent protein (CFP) fused to a Golgi signal peptide on the right. The CFP signal is used to
905 confirm expression of the T-DNA. Bars= 20 μm. BiFC experiments were conducted two times with
906 similar results.
907
908
909

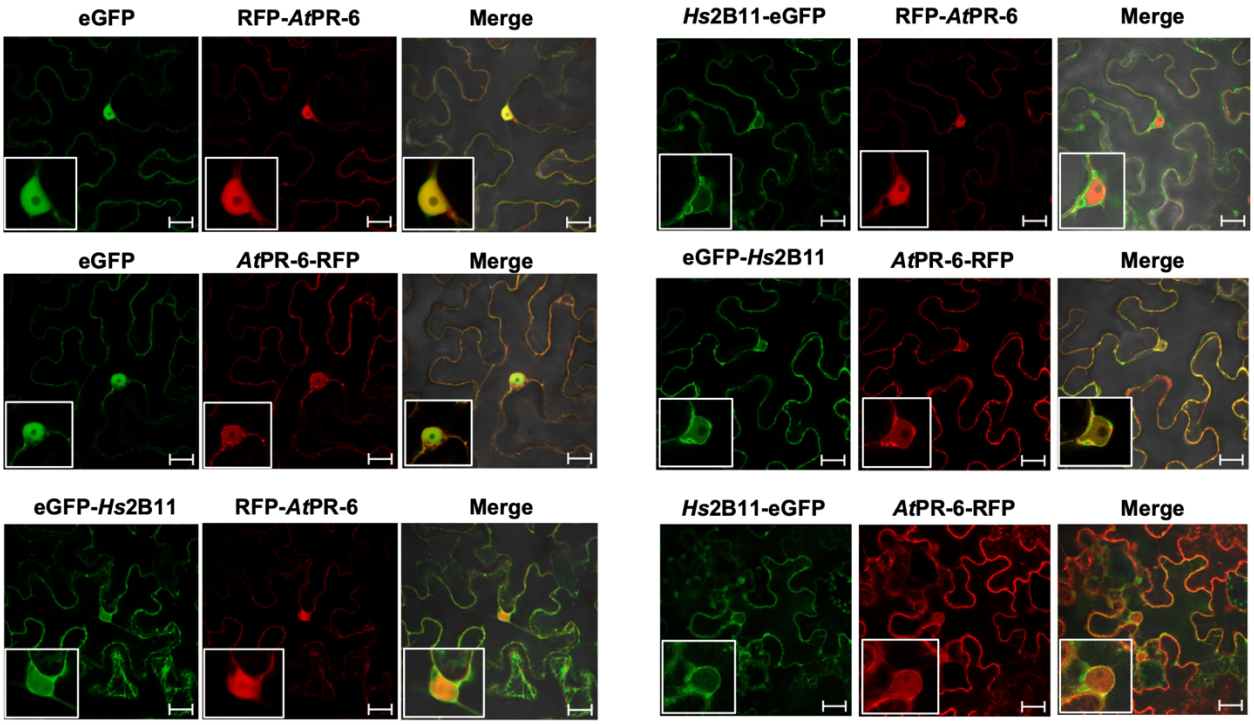

910

911 **Fig 5**. ***Hs*2B11 and *At*PR-6 co-localize in the cytoplasm and endoplasmic reticulum in *N.***
912 ***benthamiana*.** Co-localization of *Hs*2B11 and *At*PR-6, fused to eGFP and RFP, respectively.
913 eGFP alone is used as a control. Bar = 20 μM. Subcellular localization experiments were
914 conducted two times with similar results.

915

916

917

918

919

920

921

922

923

924

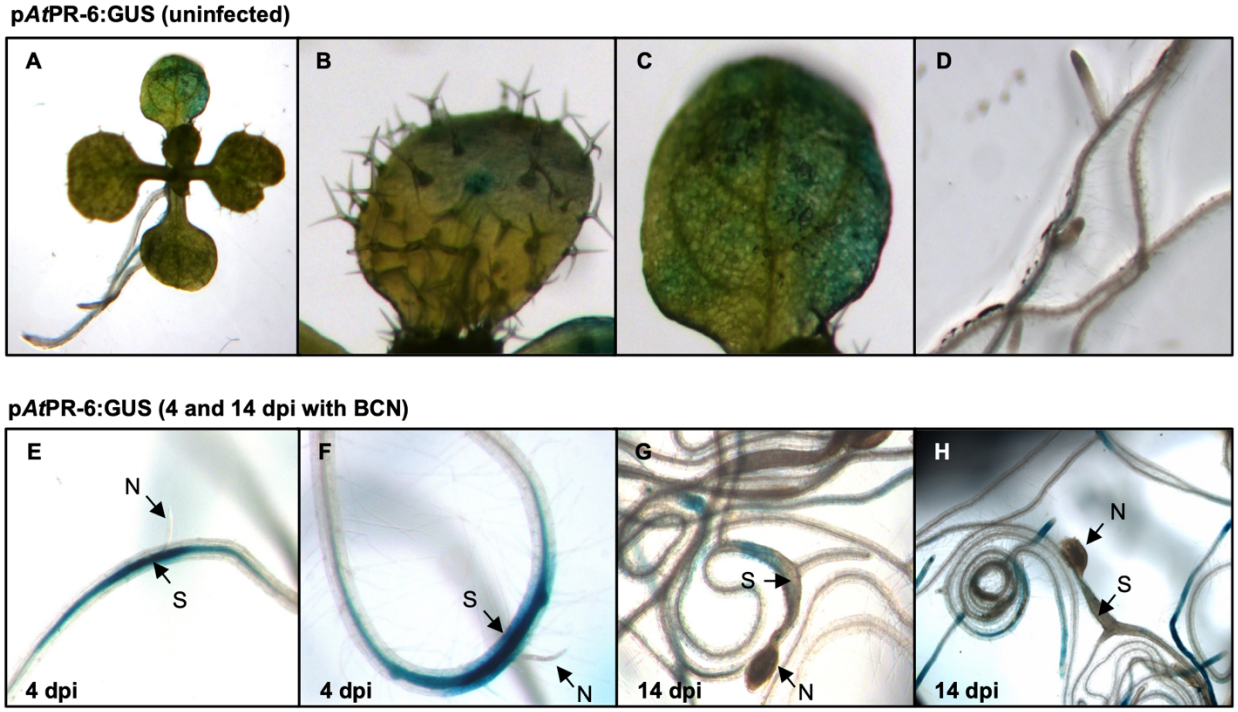

Fig 6. **Histochemical localization of GUS activity driven by the *AtPR-6* promoter.** GUS activity was observed in (A) uninfected whole Arabidopsis seedlings, (B) emerging leaves with trichomes, (C) leaves and (D) roots. *AtPR-6* promoter activity in BCN-infected Arabidopsis at 4 dpi (E-F) and 14 dpi (G,H). N= nematode; S = syncytium.

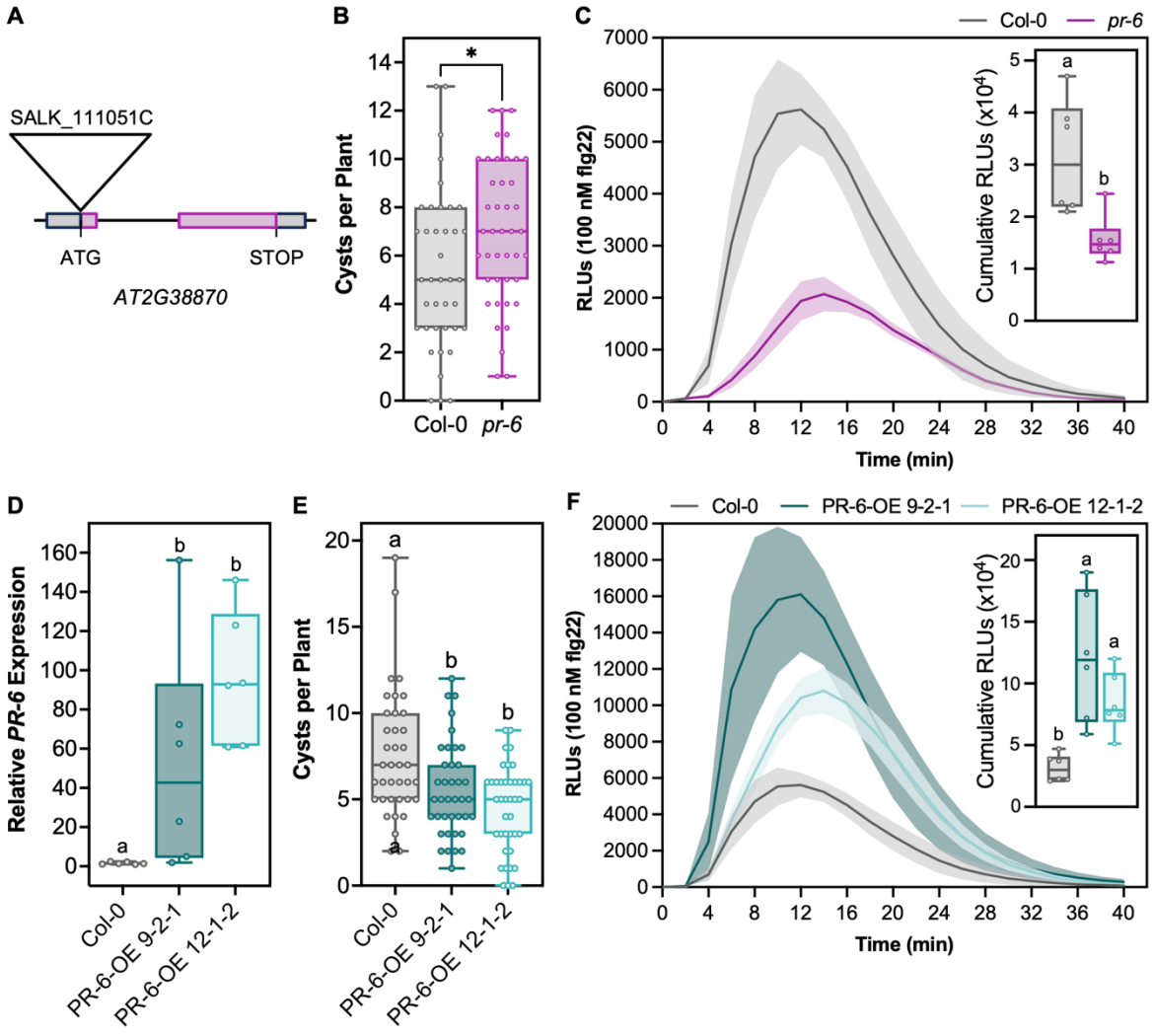

Fig 7. *At*PR-6 is a positive regulator of plant immunity and defense against *H. schachtii* infection. (A) Position of T-DNA insertion of *Atpr-6* knockout allele (Salk_111051C). (B) Number of cyst per plant in Col-0 control line and a *Atpr-6* knockout mutant 4 weeks-post infection with 250 *H. schachtii* second-stage juveniles (J2s). Data from two independent experiments are pooled. Asterisks indicate statistically significant values ($p<0.05$) as determined by a one-way analysis of variance followed by Tukey's post-hoc test. (C) Flg22-induced oxidative species production in the Arabidopsis *Atpr-6* mutant line compared to Col-0 control. Representative data from one of two experiments showing similar results are shown. (D) qRT-PCR analysis of two *AtPR-6* Arabidopsis overexpression lines. Experiments were conducted twice with similar results.

950 (E) Number of BCN cysts per plant in Col-0 controls and two *At*PR6 overexpressing lines, 4
951 weeks-post-infection with 250 *H. schachtii* J2s. (F) ROS burst kinetics in two *At*PR-6
952 overexpression lines compared to Col-0 controls, after being challenged with flg22.
953 Representative data from one of two experiments with similar results are shown. Box plots display
954 interquartile range (25th to 75th percentile) split by a mean line. Whiskers represent maximum
955 and minimum values. Unless indicated otherwise, statistically significant values ($p<0.05$) are
956 indicated by different lowercase letters as determined by a one-way analysis of variance followed
957 by Tukey's post-hoc test.

958

959

960

961

962

963

964

965

966

967

968

969

970

971

972

973

974 ## Supporting Information Captions

975

976 **Fig S1. Expression analysis and structural modeling of *Hs*2B11 paralogs. (**A) RNA-seq
977 expression data from [25] showing the expression of four *Hs*2B11 paralogs during the life cycle
978 of whole *H. schachtii* nematodes. (B) RNA-seq expression data from [26] showing the dorsal
979 gland expression in pre-parasitic J2 (ppJ2), parasitic J2 (pJ2) and parasitic J3 (pJ3) nematodes.
980 (C) 3D structure of *Hs*2B11 paralogs as predicted by AlphafoldII (ColabFold). The N-terminus is
981 indicated in blue and the C-terminus in grey. The alignment of serines or the alternance of acid
982 and basic amino acids are displayed in purple and turquoise, respectively.

983

984 **Fig S2**. **Structural modeling and gene expression analysis of *At*PR-6 genes during BCN
985 infection.** (A) AlphaFold II predictions of the six *At*PR-6 genes. (B) RNA-seq expression data
986 from [25] showing the expression of the six *At*PR-6 genes during the life cycle of *H. schachtii*
987 nematodes.

988

989 **Fig S3**. **Yellow fluorescent protein (YFP) confocal images of BiFC experiments in *N.
990 benthamiana* epidermal cells.** (A) Empty YFPc vectors and YFPn *Hs*2B11 and (B) the C-
991 terminal fragment of *Hs*2B11, tagged with YFPn and YFPc-tagged *At*PR6. Bars=10 or 20 µm as
992 indicated in the figures. Cyan fluorescent protein (CFP) fused to a Golgi signal peptide on the
993 right. The CFP signal is used to confirm expression of the T-DNA even in the absence of YFP
994 fluorescence.

995

996 **Fig S4**. ***Hs*2B11 and *At*PR-6 interact in the ER in *N. benthamiana* epidermal cells**. Co-
997 localization of YFPn-*Hs*2B11 and *At*PR-6-YFPc or YFPc-*At*PR-6 and the ER marker *At*WAK2-

998 mCherrry-HDEL. Bars=10 or 20 μm as indicated in the figures. Cyan fluorescent protein (CFP)
999 fused to a Golgi signal peptide is used to confirm expression of the T-DNA insert.

1000

1001 **Fig S5. Histochemical localization of GUS activity controlled by the *AtPR6* promoter in**
1002 **Arabidopsis after a 4 h incubation with X-Gluc at 37°C.** GUS activity controlled by *AtPR6*
1003 promoter in uninfected whole (A) Arabidopsis seedlings, (B) leaves (C) emerging leaves with
1004 trichomes, and (D-E) roots.

1005

1006 **Table S1. Y2H summary using *At*PR-6 as a bait.**

1007

1008 **Table S2. Primers used in this study.**